Bending-Induced Symmetry Breaking of Lithiation in Germanium Nanowires

Meng Gu,[†,#] Hui Yang,[‡,#] Daniel E. Perea,[†] Ji-Guang Zhang,[§] Sulin Zhang,*[,‡] and Chong-Min Wang*[,†]

[†]Environmental Molecular Sciences Laboratory and [§]Energy and Environmental Directorate, Pacific Northwest National Laboratory, 902 Battelle Boulevard, Richland, Washington 99352, United States

[‡]Engineering Science and Mechanics and Bioengineering, Pennsylvania State University, University Park, State College, Pennsylvania 16801, United States

Ⓢ *Supporting Information*

ABSTRACT: From signal transduction of living cells to oxidation and corrosion of metals, mechanical stress intimately couples with chemical reactions, regulating these biological and physiochemical processes. The coupled effect is particularly evident in the electrochemical lithiation/ delithiation cycling of high-capacity electrodes, such as silicon (Si), where on the one hand lithiation-generated stress mediates lithiation kinetics and on the other the electrochemical reaction rate regulates stress generation and mechanical failure of the electrodes. Here we report for the first time the evidence on the controlled lithiation in germanium nanowires (GeNWs) through external bending. Contrary to the symmetric core−shell lithiation in free-standing GeNWs, we show bending the GeNWs breaks the lithiation symmetry, speeding up lithaition at the tensile side while slowing down at the compressive side of the GeNWs. The bending-induced symmetry breaking of lithiation in GeNWs is further corroborated by chemomechanical modeling. In the light of the coupled effect between lithiation kinetics and mechanical stress in the electrochemical cycling, our findings shed light on strain/stress engineering of durable high-rate electrodes and energy harvesting through mechanical motion.

KEYWORDS: Ge nanowires, Li ion battery, in situ TEM, symmetry breaking, chemomechanical modeling
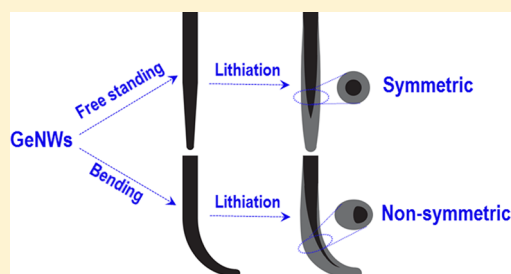
Insertion of secondary species into solid electrodes constitutes the primary energy-storage mechanism for modern battery systems.[1−4] Understanding the insertion-induced chemomechanical degradation of the host materials has become a central focus of the present battery research.[5−12] Much like other physiochemical processes such as oxidation and corrosion in metals, the electrochemical cycling of electrodes features intimate coupling between insertion kinetics and mechanical stress: the insertion of the secondary species generates localized stress, which in turn mediates electro-chemical insertion rates.[13−17] This coupled effect is particularly strong in high-capacity electrodes in which a large amount of secondary species are inserted and extracted during electro-chemical cycling. As a well-studied example, crystalline silicon (c-Si), a negative electrode material with a theoretical capacity 10-fold higher than graphite,[18−20] undergoes ∼300% volume expansion and generates large localized tensile stress on its surface during electrochemical lithiation,[7] leading to size-dependent surface fracture.[8,14] Reciprocally, lithiation induced mechanical stress causes retardation or even arrest of lithiation.[13,14] Understanding the coupled effect is therefore imperative for capacity retention and cycle life extension of the high-rate lithium ion batteries (LIBs).

While the coupled effect in the electrochemical cycling of electrodes has long been recognized, the strong effect of the electrochemical reaction rate on the degradation of electrode

materials has only been recently appreciated through the distinctly different lithiation behaviors of crystalline germanium (c-Ge) and c-Si.[12] Ge, another Li-alloying negative electrode material with a high capacity (1384 mAhg^{-1}) second only to Si,[20] undergoes ∼260% volume increase (i.e., the volume of the fully lithiated product is ∼360% of the original structure) upon full lithiation.[12] Both the electron conductivity and the Li diffusivity in Ge are much higher than those in Si,[21,22] rendering Ge an attractive high-rate electrode material.[23−29] Recent in situ transmission electron microscopy (TEM) studies revealed that lithiation of both c-Si and c-Ge proceeds by the motion of an atomically sharp two-phase interface: the lithiated amorphous phase progressively consumes the crystalline phase, forming a core−shell structure.[7,12,30] Differently, the electrochemical lithiation rate in c-Si is crystallographic orientation depend-ent,[7,31,32] as opposed to the isotropic lithiation in c-Ge,[12] despite the similar crystalline structures of these two crystals. Consequently, c-Si undergoes anisotropic swelling, leading to crack nucleation and growth at well-defined angular sites of the outer surface of the Si crystals,[10,12,14] in distinct contrast to the isotropic swelling and tough behavior of c-Ge throughout the entire lithiation process.[12] The same correlation between
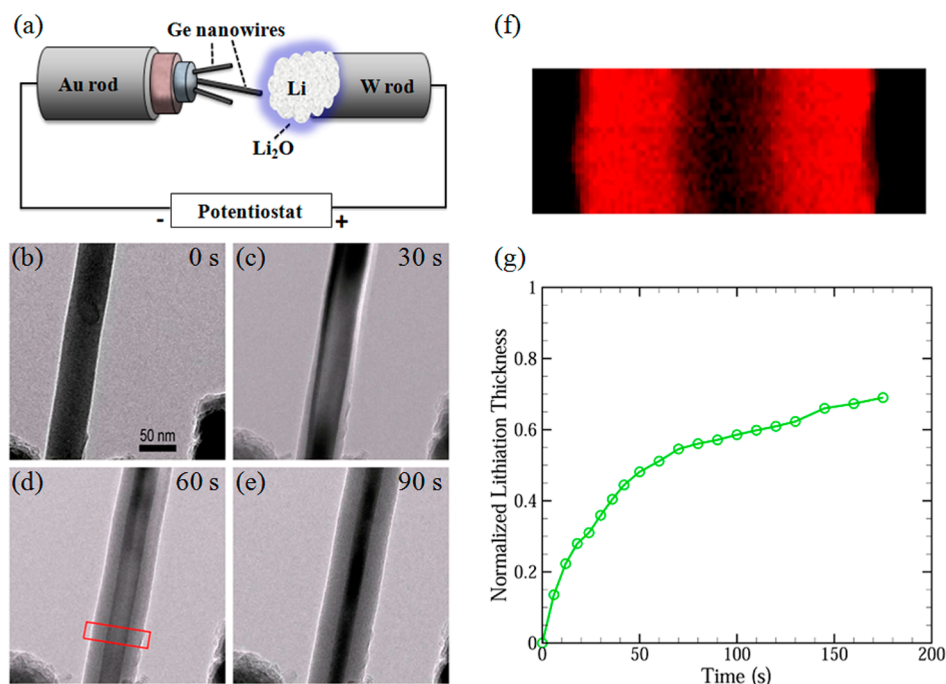
Figure 1. Morphological evolution of a free-standing GeNW under lithiation. (a) Schematics of the in situ nanobattery setup, consisting of a single GeNW as the working electrode, bulk Li as the counter electrode, and a native Li_2O surface layer on the Li metal as the solid electrolyte. (b) A pristine c-GeNW with a diameter of 50 nm. (c–e) TEM snapshots showing the uniform lithiation in the radial direction, forming core–shell structures. (f) Li distribution map obtained by EELS mapping at the region marked by the red rectangle in d; the dark region corresponds to the crystalline core of the cross section. (g) Time-dependent lithiation thickness of the free-standing c-GeNW, showing lithiation retardation due to the lithiation-generated stress.

isotropic lithiation and high toughness was recently observed in amorphous Si,[33] further demonstrating the critical role of the lithiation rate anisotropy on the degradation of the electrodes. The rate-dependent chemomechanical behavior suggests that controlling the electrochemical reaction rate represents a new pathway for the design of durable high-capacity LIBs.

Using in situ TEM studies, we demonstrate in this work the control of the lithiation rate in GeNWs by the external bending. The GeNWs used in this study were grown using chemical vapor deposition (CVD), which has been widely used to fabricate SiNWs. The GeNWs were doped with phosphorus for enhanced electrical conductivity. The diameter of the GeNWs ranges from 50 to 220 nm and the length from 2 to 10 μm. The in situ TEM was carried out based on an open-cell nanobattery configuration, which consists of a single GeNW as the working electrode, bulk Li as the counter electrode, and a native Li_2O surface layer grown on the Li metal as the solid electrolyte, as schematically shown in Figure 1a. The nanobattery device was implanted in TEM using a Nanofactory scanning tunneling microscopy (STM) holder. An overpotential ranging from −0.5 to −2 V was applied to drive the Li ions across the Li_2O solid electrolyte for lithiation. The in situ TEM study enables real-time imaging of electrochemical reactions in GeNWs.

Figures 1b–e show the TEM images of a free-standing c-GeNW with an initial diameter of 50 nm at different lithiation stages. As soon as the Li metal touched the GeNW (Figure 1b), Li quickly diffused over a long distance along the GeNW surface within several seconds before bulk lithiation in the radial direction occurred (see Figure 1c and Movie S1 in Supporting Information), owing to the much higher Li diffusion rate on the surface than in the bulk of Ge, similar to the lithiation of Si.[7,12–14,33,34] The GeNW then started to expand (Figure 1d)

radially, indicative of bulk lithiation, forming a structure consisting of a c-Ge core and a lithiated shell of amorphous Li_xGe (a-Li_xGe). Similar core–shell structures have been widely observed in lithiated SiNWs and Si nanoparticles (SiNPs).[7,8,14,30,33] Previous studies revealed that lithiation of c-Ge proceeds by a two-step phase transformation: (c-Ge → a-Li_xGe → c-$Li_{15}Ge_4$).[12,35] The volume increase of the free-standing c-GeNW due to lithiation was measured to be ∼260%, which is consistent with previous studies,[12] indicating that the lithiated product was likely to be c-$Li_{15}Ge_4$. These structural observations are also corroborated by the spatial distribution of Li probed by the electron energy loss spectroscopy (EELS) (Figure 1(f)). We noted that lithiation proceeded in an axisymmetric manner in the radial directions at any axial positions, in contrast to the orientation dependent lithiation in c-Si.[7,31,32] As a result, the unlithiated core should be of the circular shape for all of the cross sections. Throughout the lithiation process, the GeNW remained straight, indicative of minimal axial stress imposed to the nanowire during the lithiation process.

We observed that the thickness of the lithiated shell at a given lithiation time was nearly the same at different axial positions, further demonstrating a much higher surface diffusivity of Li than the bulk diffusivity. Thus, the cross sections of c-GeNW at any different axial locations were lithiated in a similar manner. Figure 1g plots the time-dependent lithiation thickness at a representative cross section of the c-GeNW, where the slope of the curve indicates the lithiation rate. The plot shows that the lithiation started rather fast (∼1.13 nm/s), but gradually slowed down (∼0.06 nm/s) as lithiation proceeded, exhibiting lithiation retardation. Similar lithiation retardation behavior has been previously observed in
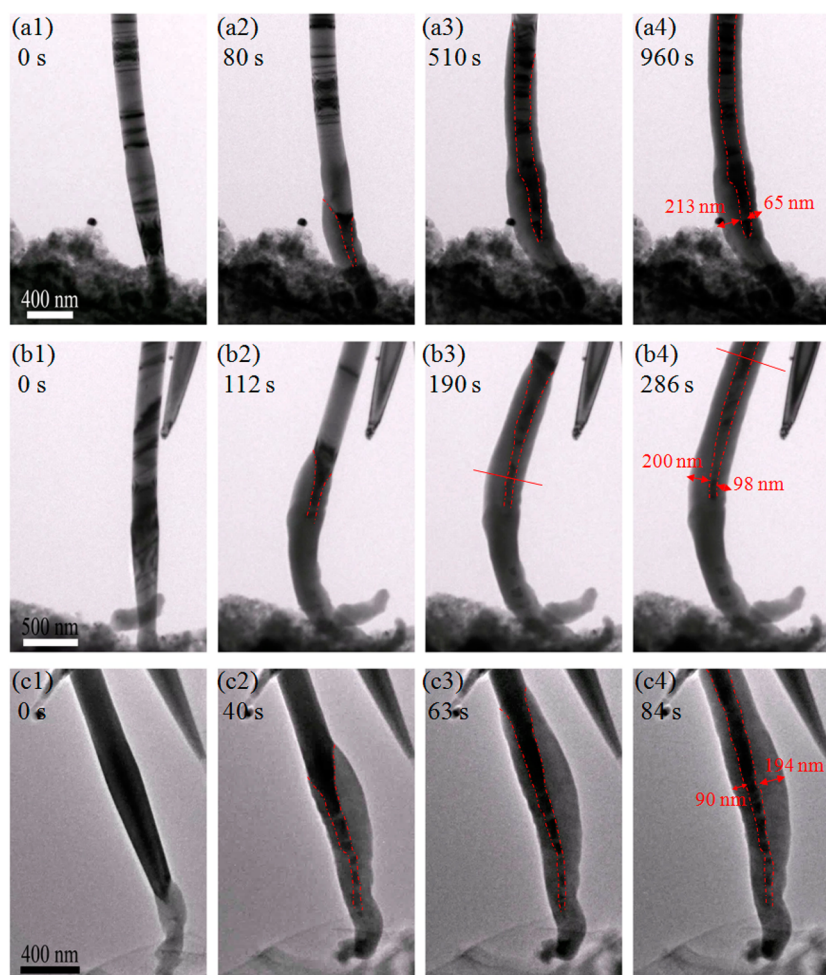
Figure 2. TEM snapshots showing the symmetry-breaking in lithiation of three representative GeNWs. The GeNWs were pushed against the Li metal to create bending during the lithiation processes, leading to lithiation asymmetry. The unlithiated crystalline cores in the GeNWs are outlined by the dashed red lines. Panels A and B: the GeNWs were pushed to the left. Panel C: the GeNW was pushed to the right.

c-SiNPs and c-SiNWs[13,14] and has been understood as a result of suppressed lithiation rate and Li diffusion due to the lithiation self-generated compressive stress at the reaction front and in the lithiated shell, respectively.

On the basis of the coupled effect of the mechanical stress and the electrochemical lithiation rate, an externally applied load might also mediate the electrochemical lithiation rate in the same manner as lithiation self-generated stress in the GeNWs. To see this, the GeNWs were brought into contact with the Li metal for lithiation. As soon as lithiation started, the GeNWs were pushed against the Li metal electrode using a piezoelectric nanomanipulator, as shown in Figure 2. The pushing force effectively bent the GeNWs while the GeNWs were being lithiated, generating a complex stress state in the GeNWs with the mixed components of bending and axial compression. The stress profile is thus radially nonuniform in the bent region such that one side of the GeNW undergoes compression and the other undergoes tension. Owing to the axial compression, the neutral plane is not the central plane of the GeNW but shifted to the tensile side. Panel A of Figure 2 (and Movie S2 in Supporting Information) displays an initially tapered GeNW (Figure 2a1) pushed to the left (i.e., the tensile side is on the left) during lithiation. The diameter of the uniform portion of the GeNW is ~220 nm. The dark contours shown in Figures 2a1−a2 correspond to the strain induced

diffraction contrast. Lithiation of the bent GeNW also generated a core−shell structure (Figures 2a2−a4), similar to the free-standing GeNW, where the red dashed lines mark the boundaries between the a-Li$_x$Ge shell and the c-Ge core. However, the reaction front propagated asymmetrically on the tensile and compressive sides, with a noticeably higher lithiation rate on the tensile side than the compressive side. As a result, the radially uniform core−shell structure observed in the free-standing GeNW was broken in the bent GeNW. As lithiation continued, the constraint to the volume expansion along the axial direction generated increasingly higher compressive stress, which, together with the lithiation self-generated compressive stress at the reaction front, resisted further lithiation. When the combined compressive stress reached a critical value, lithiation of the GeNW was completely arrested, leaving an unlithiated core in the GeNW. This asymmetric lithiation resulted in a nonuniform core−shell structure, featuring a thicker lithiated shell (~213 nm) on the tensile side and thinner on the compressive side (~65 nm) at the bent region, as shown in Figure 2a4. It should be noted that bending-induced nonuniform contact conditions between the GeNW and the Li source biased the Li diffusion distance from the Li source to the tensile and compressive sides. However, this small biased distance should not be responsible for the symmetry-breaking of lithiation observed in the experiments since surface diffusion

C

dx.doi.org/10.1021/nl501680w | Nano Lett. XXXX, XXX, XXX−XXX

of Li is much faster, making the time scale associated with the biased distance negligibly small. We repeated the bending experiments with other GeNWs, and similar results were observed, as shown in panels B and C of Figure 2 and the associated movies (see Movies S3 and S4) in the Supporting Information. In panel B, the GeNW with a diameter of ∼220 nm was pushed to the left, and its lithiation morphology was similar to the GeNW in panel A. As lithiation came to a complete stop, the lithiated thicknesses on the tensile and compressive sides were 200 nm and 98 nm, respectively. In panel C, the GeNW with a diameter of ∼200 nm was pushed to the right, and correspondingly, lithiation proceeded at a much higher rate along the right side than the left side of the nanowire, as shown in Figures 2c2, c4. At the end of lithiation, a small unreacted core remained on the left side of the nanowire. At the snapshot of 84 s, the lithiated thickness on the left side is 90 nm, compared to the 194 nm thickness on the right side.

To further appreciate the stress effects on the lithiation kinetics, we extracted the time-dependent thickness of the lithiated shells in the GeNWs. It should be noted that the lithiation kinetics may depend on the diameter of the GeNWs, the doping conditions, the extent of pushing, and the applied overpotential, all of which may vary for different GeNWs, rendering direct comparisons of the lithiation kinetics infeasible for different GeNWs. Hence, our analysis below will be focused on the general trend of the stress effects on the lithiation kinetics.

Figure 3 plots the time-dependent normalized thickness of the lithiation shell for the bent GeNWs. The thickness is
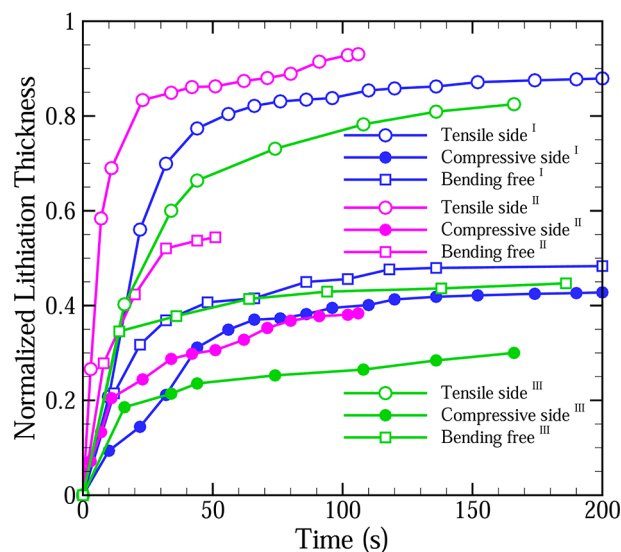
Figure 3. Time-dependent normalized lithiation thickness of the bent GeNWs (I: the GeNW shown in panel B in Figure 2; II: the GeNW shown in panel C in Figure 2; and III: the GeNW shown in Movie S5 in the Supporting Information). The thickness is normalized by the diameter of the corresponding pristine GeNW.

normalized by the diameter of the corresponding pristine GeNW. For each GeNW, we chose two distinct cross sections at different axial positions, one located at the highly curved point and the other at the straight portion (bending free) of the GeNW, as marked, for instance, in Figures 2b3, b4, respectively. Owing to the symmetry breaking at the curved segment, we plot the lithiated thicknesses of the tensile and compressive sides separately. From all three curves associated with the bent

GeNW, lithiation started with a relatively high speed (>2.5 nm/s) and slowed down gradually to a rather low speed (<0.1 nm/s). The initial lithiation rate for the tensile side of the cross section of the bent point is the highest, manifested by the steepest slope of the curves. The data points for the straight point fell between those for the tensile and compressive sides, indicating an intermediate stress state of this cross section. We note that the curve for the straight point is closer to that for the compressive side of the curved cross section, indicating that the GeNW globally underwent axial compression. Furthermore, after a fast lithiation regime, the lithiation kinetics curves for all three cross sections become flat, indicating strong lithiation retardations. By comparison, lithiation retardation in the bent GeNW is apparently stronger than that of the free-standing GeNW since the pushing force also generated considerable axial compression in the bent GeNW.

For a quantitative understanding of the bending induced symmetry breaking in the lithiation rate in GeNWs, we extend a recently developed chemomechanical model to simulate the lithiation process in the GeNWs.[36,37] In the model, a sharp reaction front (interfacial domain) with an abrupt change of Li concentration from 0 (c-Ge) to 1 (c-Li$_{15}$Ge$_4$) is generated by adopting a concentration dependent Li diffusivity: $D = D_0 [1/(1 - c) - 2\alpha c]$, where D_0 is the diffusion constant of Li in Ge and α is a tunable constant to control the concentration profile near the reaction front. The model identifies three computational subdomains: the lithiated shell and unlithiation crystalline core, separated by the sharp two-phase interfacial domain. Since GeNWs undergo nearly isotropic lithiation, D_0, is set to be orientation-independent within the interfacial domain. Moreover, Li diffusivity on the surface of GeNWs is set to be 2 orders of magnitude larger than that in the bulk, which reflects the much faster surface diffusion than that in the bulk of GeNWs. To incorporate the stress effects in the lithiation kinetics, both the reaction rate at the reaction front and the diffusivity in the lithiated region is set to be stress-dependent, i.e., $D_{eff} = De^{-p\Omega/k_B T}$, where D_{eff} is the effective diffusivity, Ω is the activation volume of Li diffusion, $k_B T$ is the thermal energy, and p is the hydrostatic pressure that can be obtained from the trace of the Cauchy stress tensor.

The interfacial domain separates the unlithiated, elastic c-Ge core and the lithiated c-Li$_{15}$Ge$_4$ shell that undergoes large-plastic deformation. The total strain ε_{ij} in the chemomechanical model consists of three parts, $\varepsilon_{ij} = \varepsilon_{ij}^e + \varepsilon_{ij}^p + \varepsilon_{ij}^c$. That is, ε_{ij}^e is the elastic strain, ε_{ij}^p is the plastic strain, and ε_{ij}^c is the lithiation-induced electrochemical strain given by $\varepsilon_{ij}^c = \beta \delta_{ij} c$, where c denotes the local normalized Li concentration with $c = 1$ representing the Li$_{15}$Ge$_4$ phase, while $c = 0$ the pure Ge phase, β the expansion coefficient, and δ_{ij} is the Kronecker delta ($\delta_{ij} = 1$ for $i = j$, and $\delta_{ij} = 0$ otherwise). We set $\beta = 0.54$ in accordance to the ∼260% volume increase in Ge due to lithiation. To simulate the dynamic evolution of the core−shell structure in the lithiated GeNWs, the Li diffusion equation is coupled with the mechanical equilibrium equations within the framework of elastoplasticity. The Young's modulus and yield stress are set to be Li concentration dependent, varying from 130 to 30 GPa and from 1.0 to 0.2 GPa, respectively.[38−40] The coupled chemomechanical model is implemented in the finite element package ABAQUS,[41] as detailed in the Supporting Information.

A series of sequential snapshots of the simulated GeNWs during lithiation under external loading are displayed in Figure 4. Figures 4a1−a5 show the Li concentration profiles at different lithiation stages, while Figures 4b1−b5 are the
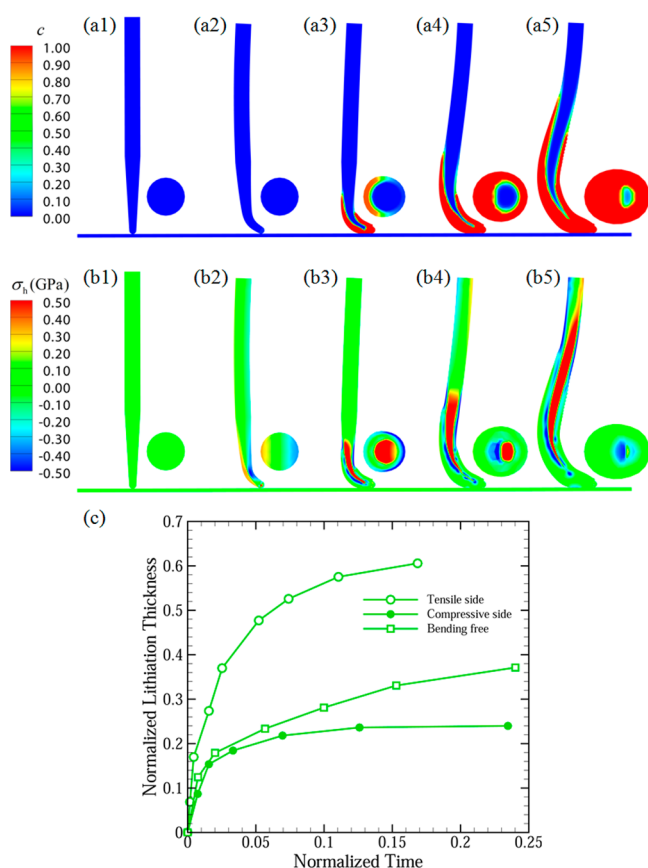
Figure 4. 3D chemomechanical modeling of the lithiation kinetics and stress generation in a GeNW subject to bending. (a1–a5) The Li concentration profiles at different lithiation stages; (b1–b5) the corresponding hydrostatic stress concentration profiles. The symmetry breaking in lithiation is clearly shown by both the longitudinal and cross-sectional views of the Li concentration and stress profiles. (c) Lithiation kinetics of the simulated GeNW. The lithiation thickness is normalized by the diameter of the simulated GeNW, and the time is normalized by the total time for the cross section to be fully lithiated.

corresponding hydrostatic stress profiles, $\sigma_h = \mathrm{tr}(\boldsymbol{\sigma})/3$, where $\mathrm{tr}(\boldsymbol{\sigma})$ is the trace of the Cauchy stress tensor $\boldsymbol{\sigma}$. To better show the bending induced symmetry breaking in lithiation, the Li concentration profile and the stress distribution of the cross section at the point of the largest curvature are also plotted at different lithiation stages. The numerically predicted morphological evolution of the GeNW during the lithiation processes under the externally applied loadis available in the Supporting Information (Movie S6). To mimic the boundary conditions in the experiments, a rigid substrate is placed at the tapered end of the GeNW, and the bottom tip of the GeNW is fully covered by Li, i.e., $c = 1$. Starting from the pristine c-GeNW (Figures 4a1, b1), axially applied external force bends the GeNW (Figures 4a2, b2), resulting in tension on the left side and compression on the right side at the bent region. The top-left corner is also compressed as a result of the pushing. Figures 4a2–a5 show the dynamic Li transport in the axial and radial directions of the GeNW, with the red color representing the nearly fully lithiated phase (c-Li$_{15}$Ge$_4$) and blue the c-Ge phase. As the Li diffusivity on the surface of the GeNW is much higher than that in the bulk, the surface of the GeNW acts as a fast Li transport path. It follows that the Li always covers the surface of the GeNW first, then flows radially inward, forming a core–

shell structure separated by a sharp interface, marked by the transition color between red and blue.

Figures 4b2–b5 plot the corresponding stress profiles at different lithiation stages. It should be noted that the resulting stress profile in the GeNW is a superimposition of the lithiation-generated stress and that caused by the external pushing force. Similar to the lithiated free-standing SiNWs, the unlithiated core undergo tension, while the two-phase interface undergoes compression (see Figures 4b3–b5),[36,37] indicating that the lithiation-generated stress dominates the stress profiles of the core-interphase in the GeNW, whereas the applied bending mostly influences the stress profile of the outer and inner surface layers at the highly curved regions. As the hydrostatic compression retards both reaction and diffusion while hydrostatic tension enhances them, the symmetry of lithiated pattern observed in bending-free GeNW is broken by bending, as shown in both the longitudinal review and the cross-sectional view. Consequently, the lithiation proceeds appreciably faster on the left side (tension side) than on the right side (compression side) of the GeNW in both radial and axial directions. Therefore, an asymmetrical core–shell is generated, as shown by the Li concentration profile of the cross section at the bent region in Figure 4. At the end of the lithiation (Figures 4a5, b5), the cross section become elliptically shaped with an unlithiated core being located closer to the compressive side, further demonstrating the symmetry breaking in the lithiation process. The lithiation kinetics in the simulated GeNW is shown in Figure 4c. Compared with Figure 3, these curves show the same trends: lithiation started with a very high speed and slowed down gradually, illustrating the consistence between theoretical and experimental results.

In summary, we investigate the influence of the external bending on the lithiation kinetics and deformation morphologies in GeNWs. It was found that free-standing GeNWs undergo isotropic lithiation. Lithiation self-generated internal stress due to the incompatible strain at the reaction front causes lithiation retardation in the free-standing GeNWs, similar to SiNWs and SiNPs. Bending a GeNW during lithiation breaks the lithiation symmetry, enhancing the lithiation rate on the tensile side while suppressing it on the compressive side, both in the radial and the axial directions. Chemomechanical modeling corroborates the experimental observations and suggests the stress dependence of both Li diffusion and interfacial reaction rate during lithiation.

The external load mediated lithiation kinetics opens new pathways to improve the performance of electrode materials by tailoring lithiation rate via strain engineering. As anisotropic lithiation constitutes the primary origin for the fracture of c-Si,[12] external forces, such as bending, might be applied to suppress the lithiation anisotropy, therefore mitigating fracture. Our findings also suggest that pretension may counteract with the self-generated compressive stress in the electrodes during lithiation, thereby improving the rate performance of the LIBs. Moreover, as an electrode is of essentially multicomponents, local mechanical incompatibility among different components, particularly due to the large volume expansion of the high-capacity active materials, generates highly localized compressive stress that may subsequently result in poor rate performance and capacity loss of the battery. Therefore, active materials should be appropriately spaced such that certain extent of free expansion is permitted to avoid buildup of high compressive stresses. Furthermore, in the light of bending-induced symmetry breaking of lithiation and considering a thin-film

structure with preinserted secondary species(hydrogen, Li, Na, etc.), bending of the thin film modifies the chemical potentials of the secondary species, leading to the flux of the inserted species from the compressive side to the tensile side. The mechanically controlled flux of the secondary species features a novel energy harvesting mechanism through mechanical stress.

■ ASSOCIATED CONTENT

ⓢ Supporting Information

In situ TEM lithiation movies and chemomechanical simulation details. This material is available free of charge via the Internet at http://pubs.acs.org.

■ AUTHOR INFORMATION

Corresponding Authors
*E-mail: (S.L.Z.) suz10@psu.edu.
*E-mail: (C.M.W.) Chongmin.Wang@pnnl.gov.

Author Contributions
#M.G. and H.Y. contributed equally to this work.

Notes
The authors declare no competing financial interest.

■ ACKNOWLEDGMENTS

■ REFERENCES

(1) Tarascon, J. M.; Armand, M. Nature 2001, 414 (6861), 359−367.
(2) Cairns, E. J.; Albertus, P. Batteries for Electric and Hybrid-Electric Vehicles. In Annual Review of Chemical and Biomolecular Engineering, Vol. 1; Prausnitz, J. M., Doherty, M. F., Segalman, M. A., Eds.; Annual Reviews: Palo Alto, CA, 2010; Vol. 1, pp 299−320.
(3) Service, R. F. Science 2011, 332 (6037), 1494−1496.
(4) Liu, C.; Li, F.; Ma, L. P.; Cheng, H. M. Adv. Mater. 2010, 22 (8), E28−E62.
(5) Arico, A. S.; Bruce, P.; Scrosati, B.; Tarascon, J.-M.; van Schalkwijk, W. Nat. Mater. 2005, 4 (5), 366−377.
(6) Beaulieu, L. Y.; Eberman, K. W.; Turner, R. L.; Krause, L. J.; Dahn, J. R. Electrochem. Solid State Lett. 2001, 4 (9), A137−A140.
(7) Liu, X. H.; Zheng, H.; Zhong, L.; Huang, S.; Karki, K.; Zhang, L. Q.; Liu, Y.; Kushima, A.; Liang, W. T.; Wang, J. W.; Cho, J.-H.; Epstein, E.; Dayeh, S. A.; Picraux, S. T.; Zhu, T.; Li, J.; Sullivan, J. P.; Cumings, J.; Wang, C.; Mao, S. X.; Ye, Z. Z.; Zhang, S.; Huang, J. Y. Nano Lett. 2011, 11 (8), 3312−3318.
(8) Liu, X. H.; Zhong, L.; Huang, S.; Mao, S. X.; Zhu, T.; Huang, J. Y. ACS Nano 2012, 6 (2), 1522−1531.
(9) Liu, Y.; Zheng, H.; Liu, X. H.; Huang, S.; Zhu, T.; Wang, J.; Kushima, A.; Hudak, N. S.; Huang, X.; Zhang, S.; Mao, S. X.; Qian, X.; Li, J.; Huang, J. Y. ACS Nano 2011, 5 (9), 7245−7253.
(10) Lee, S. W.; McDowell, M. T.; Berla, L. A.; Nix, W. D.; Cui, Y. Proc. Natl. Acad. Sci. U.S.A. 2012, 109 (11), 4080−4085.

(11) Liang, W.; Hong, L.; Yang, H.; Fan, F.; Liu, Y.; Li, H.; Li, J.; Huang, J. Y.; Chen, L.-Q.; Zhu, T.; Zhang, S. Nano Lett. 2013, 13 (11), 5212−5217.
(12) Liang, W.; Yang, H.; Fan, F.; Liu, Y.; Liu, X. H.; Huang, J. Y.; Zhu, T.; Zhang, S. ACS Nano 2013, 7 (4), 3427−3433.
(13) Liu, X. H.; Fan, F.; Yang, H.; Zhang, S.; Huang, J. Y.; Zhu, T. ACS Nano 2012, 7 (2), 1495−1503.
(14) McDowell, M. T.; Ryu, I.; Lee, S. W.; Wang, C.; Nix, W. D.; Cui, Y. Adv. Mater. 2012, 24 (45), 6034−6041.
(15) Yang, H.; Huang, X.; Liang, W.; van Duin, A. C. T.; Raju, M.; Zhang, S. Chem. Phys. Lett. 2013, 563 (0), 58−62.
(16) Huang, X.; Yang, H.; Liang, W.; Raju, M.; Terrones, M.; Crespi, V. H.; van Duin, A. C. T.; Zhang, S. Appl. Phys. Lett. 2013, 103 (15), 153901−4.
(17) Grantab, R.; Shenoy, V. B. J. Electrochem. Soc. 2012, 159 (5), A584−A591.
(18) Kasavajjula, U.; Wang, C. S.; Appleby, A. J. J. Power Sources 2007, 163 (2), 1003−1039.
(19) Zhang, W. J. J. Power Sources 2011, 196 (1), 13−24.
(20) Larcher, D.; Beattie, S.; Morcrette, M.; Edstroem, K.; Jumas, J. C.; Tarascon, J. M. J. Mater. Chem. 2007, 17 (36), 3759−3772.
(21) Graetz, J.; Ahn, C. C.; Yazami, R.; Fultz, B. J. Electrochem. Soc. 2004, 151 (5), A698−A702.
(22) Chan, C. K.; Zhang, X. F.; Cui, Y. Nano Lett. 2008, 8 (1), 307−309.
(23) Lee, H.; Kim, H.; Doo, S.-G.; Cho, J. J. Electrochem. Soc. 2007, 154 (4), A343−A346.
(24) Park, M.-H.; Cho, Y.; Kim, K.; Kim, J.; Liu, M.; Cho, J. Angew. Chem. 2011, 123 (41), 9821−9824.
(25) Jo, G.; Choi, I.; Ahn, H.; Park, M. J. Chem. Commun. 2012, 48 (33), 3987−3989.
(26) Xue, D.-J.; Xin, S.; Yan, Y.; Jiang, K.-C.; Yin, Y.-X.; Guo, Y.-G.; Wan, L.-J. J. Am. Chem. Soc. 2012, 134 (5), 2512−2515.
(27) Woo, S.-H.; Choi, S. J.; Park, J.-H.; Yoon, W.-S.; Hwang, S. W.; Whang, D. J. Electrochem. Soc. 2013, 160 (1), A112−A116.
(28) Klavetter, K. C.; Wood, S. M.; Lin, Y.-M.; Snider, J. L.; Davy, N. C.; Chockla, A. M.; Romanovicz, D. K.; Korgel, B. A.; Lee, J.-W.; Heller, A.; Mullins, C. B. J. Power Sources 2013, 238 (0), 123−136.
(29) Liu, Y.; Zhang, S.; Zhu, T. ChemElectroChem. 2014, 1 (4), 706−713.
(30) Liu, X. H.; Wang, J. W.; Huang, S.; Fan, F.; Huang, X.; Liu, Y.; Krylyuk, S.; Yoo, J.; Dayeh, S. A.; Davydov, A. V.; Mao, S. X.; Picraux, S. T.; Zhang, S.; Li, J.; Zhu, T.; Huang, J. Y. Nat. Nanotechnol. 2012, 7 (11), 749−756.
(31) Lee, S. W.; McDowell, M. T.; Choi, J. W.; Cui, Y. Nano Lett. 2011, 11 (7), 3034−3039.
(32) Goldman, J. L.; Long, B. R.; Gewirth, A. A.; Nuzzo, R. G. Adv. Funct. Mater. 2011, 21 (13), 2412−2422.
(33) McDowell, M. T.; Lee, S. W.; Harris, J. T.; Korgel, B. A.; Wang, C.; Nix, W. D.; Cui, Y. Nano Lett. 2013, 13 (2), 758−764.
(34) Sun, C.-F.; Karki, K.; Jia, Z.; Liao, H.; Zhang, Y.; Li, T.; Qi, Y.; Cumings, J.; Rubloff, G. W.; Wang, Y. ACS Nano 2013, 7 (3), 2717−2724.
(35) Liu, X. H.; Huang, S.; Picraux, S. T.; Li, J.; Zhu, T.; Huang, J. Y. Nano Lett. 2011, 11 (9), 3991−3997.
(36) Yang, H.; Huang, S.; Huang, X.; Fan, F.; Liang, W.; Liu, X. H.; Chen, L.-Q.; Huang, J. Y.; Li, J.; Zhu, T.; Zhang, S. Nano Lett. 2012, 12 (4), 1953−1958.
(37) Yang, H.; Fan, F.; Liang, W.; Guo, X.; Zhu, T.; Zhang, S. J. Mech. Phys. Solids 2014, DOI: 10.1016/j.jmps.2014.06.004.
(38) Chou, C.-Y.; Kim, H.; Hwang, G. S. J. Phys. Chem. C 2011, 115 (40), 20018−20026.
(39) Roundy, D.; Cohen, M. L. Phys. Rev. B 2001, 64 (21), 212103.
(40) Smith, D. A.; Holmberg, V. C.; Korgel, B. A. ACS Nano 2010, 4 (4), 2356−2362.
(41) ABAQUS; Dassault Systemes Simulia Corp.: Providence, RI, 2010.

F

dx.doi.org/10.1021/nl501680w | Nano Lett. XXXX, XXX, XXX−XXX